^{11}C-Dihydrotetrabenazine PET of the Pancreas in Subjects with Long-Standing Type 1 Diabetes and in Healthy Controls

Robin Goland*[1], Matthew Freeby*[1], Ramin Parsey*[2], Yoshifumi Saisho[3], Dileep Kumar[2,4], Norman Simpson[2], Joy Hirsch[4], Martin Prince[4], Antonella Maffei[5,6], J. John Mann[2], Peter C. Butler[3], Ronald Van Heertum[4], Rudolph L. Leibel[1], Masanori Ichise†[4], and Paul E. Harris†[1,6]

[1]Naomi Berrie Diabetes Center, Columbia University Medical Center, New York, New York; [2]Department of Psychiatry of Columbia University Medical Center, New York, New York; [3]Larry Hillblom Islet Research Center, University of California, Los Angeles, California; [4]Department of Radiology of Columbia University Medical Center, New York, New York; [5]Institute of Genetics and Biophysics "Adriano Buzzati-Traverso," CNR, Naples, Italy; and [6]Department of Medicine of Columbia University Medical Center, New York, New York

Type 2 vesicular monoamine transporter (VMAT2), found in the brain, is also expressed by β-cells of the pancreas in association with insulin. Preclinical experiments suggested that ^{11}C-dihydrotetrabenazine PET–measured VMAT2 binding might serve as a biomarker of β-cell mass. We evaluated the feasibility of ^{11}C-dihydrotetrabenazine PET quantification of pancreatic VMAT2 binding in healthy subjects and patients with long-standing type 1 diabetes. **Methods:** ^{11}C-Dihydrotetrabenazine PET was performed on 6 patients and 9 controls. VMAT2 binding potential (BP_{ND}) was estimated voxelwise by using the renal cortex as reference tissue. As an index of total pancreatic VMAT2, the functional binding capacity (the sum of voxel BP_{ND} × voxel volume) was calculated. Pancreatic BP_{ND}, functional binding capacity, and stimulated insulin secretion measurements were compared between groups. **Results:** The pancreatic mean BP_{ND} was decreased in patients (1.86 ± 0.05) to 86% of control values (2.14 ± 0.08) ($P = 0.01$). In controls, but not in patients, BP_{ND} correlated with stimulated insulin secretion ($r^2 = 0.50$, $P = 0.03$). The average functional binding capacity was decreased by at least 40% in patients ($P = 0.001$). The changes in functional binding capacity and BP_{ND} were less than the near-complete loss of stimulated insulin secretion observed in patients ($P = 0.001$). **Conclusion:** These results suggest that ^{11}C-dihydrotetrabenazine PET allows quantification of VMAT2 binding in the human pancreas. However, BP_{ND} and functional binding capacity appear to overestimate β-cell mass given the near-complete depletion of β-cell mass in long-standing type 1 diabetes, which may be due to higher nonspecific binding in the pancreas than in the renal cortex.

Key Words: β-cell mass; diabetes; VMAT2; ^{11}C-dihydrotetrabenazine; PET

J Nucl Med 2009; 50:382–389
DOI: 10.2967/jnumed.108.054866

Received Jun. 3, 2008; revision accepted Oct. 6, 2008.
For correspondence or reprints contact: Paul E. Harris, Department of Medicine, BB 20-06, Columbia University Medical Center, 650 W. 168th St., New York, NY, 10032.
E-mail: peh1@columbia.edu
*Contributed equally to this work.
†Contributed equally to this work.

Type 1 diabetes begins when β-cells of the endocrine pancreas are destroyed by an autoimmune process. Once a threshold loss of β-cell mass is reached, the pancreas is no longer able to secrete sufficient insulin to maintain glucose homeostasis. However, our understanding of the relationship of the decline in β-cell mass to the natural history of the disease is limited, because our understanding is based largely on indirect in vivo measures of β-cell mass or on postmortem histologic studies of β-cell mass (*1,2*).

Stimulated insulin secretion capacity is currently used as an indirect measure of β-cell mass. In healthy animal models, measurements of stimulated insulin secretion correlate well with β-cell mass measurements made ex vivo (*3*). As metrics of β-cell function, however, insulin secretion measurements have limited ability to predict the development of diabetes, particularly when intercurrent metabolic or inflammatory stress (*4*) reversibly compromises β-cell function but not necessarily β-cell mass (*5*). These limitations become evident when functional measurements are used to monitor disease progression (*6*). For example, once exogenous insulin is begun at diagnosis and hyperglycemia is controlled, previously poor β-cell function recovers. Because of the slow rate of human β-cell proliferation (*2*), this remission phase is believed to reflect the reversibility of compromised β-cell function rather than recovery of lost β-cell mass (*7*). In addition, because the pancreas is a heterogeneous "hard-to-biopsy" organ, no direct measure of β-cell mass is currently available and, thus, β-cell mass cannot be distinguished from functional defects of insulin secretion.

Type 2 vesicular monoamine transporters (VMAT2), the proteins that translocate monoamines into storage vesicles, are expressed not only in the monoaminergic neurons but also in pancreatic β-cells. VMAT2 is a better marker of the integrity of the dopamine neurons than is the dopamine

transporter, because VMAT2 is resistant to regulation by drug exposure and neuronal degeneration (*8*). VMAT2 is not detectable in exocrine cells or in islet cells stained with antiglucagon or somatostatin (*9*). The close association of VMAT2 and insulin has suggested that VMAT2 might serve as a biomarker of β-cell mass (*10*) independent of the mechanics of insulin production. The function of VMAT2 in β-cells is similar to its role in the central nervous system: control of vesicular monoamine content. In β-cells, vesicular monoamines are thought to regulate insulin secretion (*11*).

Previous studies on radioligand development have identified low-molecular-weight VMAT2 ligands, including dihydrotetrabenazine, that are highly selective for VMAT2. Dihydrotetrabenazine and its analogs developed for PET are 10,000 times more selective for VMAT2 than for VMAT1 (*12*) and bind to VMAT2 with high affinity (0.5–1 nM dissociation constant) (*13,14*). ^{11}C-Dihydrotetrabenazine was developed for use in imaging VMAT2 in dopaminergic neurons within the brain (*15*), and ^{11}C-dihydrotetrabenazine brain PET studies have shown that VMAT2 binding in the brain can be quantified and may be used as a biomarker of the integrity of the presynaptic dopamine neurons with potential applications in studies of movement disorders (*16*).

Recent studies on animal models of diabetes have suggested that PET targeting of VMAT2 in the pancreas can be used as a biomarker of β-cell mass (*17*). In this ^{11}C-dihydrotetrabenazine PET study of patients with type 1 diabetes, we evaluated the feasibility of quantification of VMAT2 binding in the pancreata of healthy controls and patients predicted to be nearly devoid of β-cell mass. We also tested the hypothesis that the total pancreatic VMAT2 functional binding capacity of long-standing type 1 diabetes is markedly reduced. Finally, we determined the correlation of a β-cell functional measure, area-under-the-curve (AUC) c-peptide, with PET-based measurements of VMAT2 binding in the pancreas.

MATERIALS AND METHODS

Subjects

Fifteen subjects, consisting of patients with long-standing type 1 diabetes ($n = 6$) and healthy controls ($n = 9$), were enrolled in this study. The key inclusion criteria for controls were a fasting glucose level less than 100 mg/dL and no first-degree relative with type 2 diabetes mellitus. The demographic and laboratory data of the 9 controls and the 6 patients are summarized in Table 1. All subjects gave written informed consent for the study, which was approved by the Institutional Review Board and radiation safety committees of Columbia University.

Metabolic Testing

The subjects fasted at least 8 h before undergoing testing for mixed-meal tolerance. Before the testing, insulin was discontinued in all patients; fasting blood sugar was required to range between 70 and 200 mg/dL at the start of the test. In 5 subjects treated with continuous insulin infusion, no insulin boluses were administered within 2 h of the testing, and the basal insulin was suspended 30 min before the test. Serial samples of venous serum were assayed for glucose (mg/dL), insulin (μIU/mL), and c-peptide (ng/mL) by standard methods. The c-peptide detection limit was 0.15 ng/mL. From the c-peptide concentrations obtained at each time point during the 120-min mixed-meal tolerance testing, the AUC c-peptide was calculated by the trapezoidal rule.

TABLE 1. Demographic and Laboratory Data

Parameter	Controls ($n = 9$)	Patients ($n = 6$)	*P*
Age (y)	30.1 ± 2.9	35.0 ± 2.3	0.12
Sex (male:female)	5:4	2:4	NA†
Body mass index (kg/m^2)	23.4 ± 1.1	24.6 ± 0.8	0.22
Weight (kg)	66 ± 12	72 ± 4	0.32
Hemoglobin A1c (%)	5.1 ± 0.1	6.9 ± 0.4	<0.001
Insulin dose/d (units/kg/d)	NA	39.1 ± 4.5	NA
Duration of type 1 diabetes (y)	NA	27.3 ± 1.5	NA
Estimated glomerular filtration rate – Modification of Diet in Renal Disease Study formula (mL/min/1.73 m^2)	99.8 ± 7.8	99.2 ± 5.1	0.48

Data are mean ± SEM.
NA = not applicable.

PET Studies

^{11}C-(+)dihydrotetrabenazine was synthesized as described previously (*18*). PET data were acquired for 90 min (27 frames consisting of six 10-s, three 60-s, two 120-s, and sixteen 300-s frames) after the bolus injection of 370–740 MBq of ^{11}C-dihydrotetrabenazine (specific activity, 35–62 GBq/μmol at the time of injection, and chemical purity > 95%) on an Accel scanner (CTI-Siemens) in 3-dimensional mode (47 image planes, 16.2-cm axial field of view). After correction for attenuation, scatter, and radioactive decay, PET data were reconstructed using filtered backprojection with a Hahn filter having a cutoff frequency of 0.5, resulting in a full width at half maximum of 6.22 mm at 1 cm in the tangential plane and 5.71 mm at 1 cm in the axial plane and a total of 128 × 128 × 335 voxels (1 voxel = 0.018 mL).

Metabolite-Corrected Input Function

Four healthy subjects underwent multiple sampling of arterial blood (25 times over 90 min). Blood samples were separated into plasma and a cellular fraction by centrifugation. Selected plasma fractions ($n = 6$) were analyzed by radio–high-performance liquid chromatography as previously described (*19*). The fraction of parent radioligand in plasma was fitted to a sum of 2 exponentials. A metabolite-corrected plasma curve was generated by the product of the plasma activity and metabolite fraction curves. The portion of the metabolite-corrected plasma curve beyond the initial peak was fit to a sum of 2 exponentials. The resulting curve was used as the input function for estimation of VMAT2 binding to validate the use of the reference tissue method without the input function.

MRI Studies

MRI studies were performed for guidance on the anatomic location of the pancreas needed for the PET data analysis. Each subject was scanned on a 1.5-T TwinSpeed scanner (GE Healthcare). Four single-breath-hold sequences were used: The first was axial T2-weighted single-shot fast spin echo (echo time, 90 ms; repetition time, 645 ms). The second was axial 2-dimensional fast imaging employing steady state acquisition (FIESTA) with fat saturation (echo time, 1.7 ms; repetition time, 3.8 ms; flip angle, 70°). The third was coronal 2-dimensional FIESTA with fat saturation (echo time, 1.7 ms; repetition time, 3.8 ms; flip angle, 70°). The fourth was axial liver acquisition with volume acquisition and fat saturation (echo time, 1.6 ms; repetition time, 3.6 ms; inversion time, 7; flip angle, 15°).

Rationale for Data Analysis in PET Studies

Kinetic model–based quantification of VMAT2 binding with ^{11}C-dihydrotetrabenazine has previously been shown to be feasible for the brain (*20*). In this attempt to quantify VMAT2 binding in the human pancreas, we used a reference tissue model similar to that used for the brain but with modifications adapted to the pancreas.

The VMAT2 distribution in the target organ, pancreas, is different from that of striatum in the brain, because the pancreas contains both the exocrine and the endocrine (β-cell), as well as fat tissue. VMAT2 is predominantly expressed in the insulin-producing β-cells within islets dispersed nonuniformly throughout the pancreas (*9*). Within the brain are regions devoid of VMAT2, such as the cerebellum, which can be applied as reference tissue to quantify VMAT2 without the use of the metabolite-corrected arterial plasma input function. We chose the renal cortex as the reference tissue, because it is devoid of VMAT2 (VMAT1 is present in the renal cortex but ^{11}C-dihydrotetrabenazine is highly selective for VMAT2) (*12*). The assumption made here is that the nondisplaceable (hitherto described as nonspecific) distribution volume (V'_{ND}) times the free tissue fraction (f_{ND}) is the same in the pancreas and the reference tissue and that $f_{ND}V'_{ND}$ is similar among patients and controls.

In animal models of diabetes, β-cell mass is frequently estimated by immunohistochemistry. Serial sections of pancreas tissue stained for insulin immunoreactivity are evaluated for total pancreas area and total area of insulin-staining cells. The total β-cell mass is calculated from the product of the average fractional β-cell area and the mass of the pancreas (*21*). Because these density measurements of β-cell area are analogous to the measure of VMAT2 binding potential (BP_{ND}) provided by PET, and because of the close association between insulin and VMAT2 (*9*), we reasoned that the product of voxel BP_{ND} and voxel volume, summed over the entire pancreas region of interest (ROI) (functional binding capacity), would be an appropriate estimate of the total pancreatic VMAT2 sites and that functional binding capacity could be used as a biomarker of β-cell mass.

These considerations prompted us to evaluate voxelwise quantification of VMAT2 binding (parametric imaging) using the renal cortex as the reference tissue in order to calculate the total VMAT2 functional binding capacity of the pancreas. In addition, our preliminary ROI-based quantification analysis suggested the presence of a significant amount of VMAT2 binding signal in the pancreas of patients, as was unexpected in view of the near-complete depletion of β-cell mass in long-standing type 1 diabetes (*1*). To gain further insight, we evaluated the histogram distribution of the VMAT2 binding measurements within the pancreas.

Although anatomic delineation of the pancreas was aided by the MRI scans, respiratory motion on the PET scans made this task difficult in several subjects. For this reason, delineation of the pancreas based on the dynamic PET-image tissue segmentation was also used.

Estimation of VMAT2 Binding

VMAT2 binding in the pancreas was estimated by the 2-parameter multilinear reference tissue model (MRTM2) (*22*). MRTM2 allows voxelwise estimation of $BP_{ND} = f_{ND}B_{avail}/K_D$, which is linearly proportional to the VMAT2 density (B_{avail}), where K_D and f_{ND} are the dissociation constant and f_{ND}, respectively, and R_1 represents relative radioligand delivery ($R_1 = K_1/K'_1$, the ratio of delivery rate constants of the pancreas to renal cortex), using a VMAT2-free reference region (renal cortex) instead of arterial data.

MRTM2 parametric imaging requires a priori estimation of the reference tissue radioligand clearance rate constant, k'_2, by the 3-parameter MRTM2 estimation using the ROI time–activity curve data of the target (pancreas) and reference regions (renal cortex). These ROI definitions were aided by reference to MRI scans, the R_1 images generated by the preliminary MRTM2 imaging procedure described elsewhere (*23,24*), and a modification of algorithms that allows tissue segmentation of dynamic PET images into volumes of interest exhibiting similar temporal behavior and spatial features described previously (tissue segmentation) (*25*).

In the present study, we used the left renal cortex as the reference region. Intersubject variability in time–activity curve data was less for the left kidney than for the right because of the adjacent high liver radioactivity. In addition, left renal cortex data expressed as standardized uptake value were similar in patients and controls, with no differences in the areas under these time–activity curves between the 2 groups (206 ± 24 min vs. 203 ± 32 min, $P = 0.87$), suggesting that the nonspecific distribution volume of the left renal cortex reference region (V'_{ND}) is similar for the 2 groups.

To validate the use of MRTM2 for voxelwise estimation of BP_{ND} as applied to the current ^{11}C-dihydrotetrabenazine PET data, we also estimated BP_{ND} voxelwise by the traditional compartmental kinetic analysis using the metabolite-corrected arterial plasma function in 4 controls. MRTM2 BP_{ND} and corresponding kinetic analysis BP_{ND} were compared in a randomly selected 100 voxels in each of the 4 controls, with the relationship between the 2 sets of BP_{ND} values analyzed by linear regression. All parameter estimations, including parametric imaging, were performed using the PET data analysis software PMOD (PMOD Technologies).

VMAT2 Binding Comparison

The PET-estimated VMAT2 binding in the pancreas was compared between the patient and control groups in 3 ways. First, mean BP_{ND} values over the 3-dimensional pancreatic volume were calculated for each subject and compared. Second, the sum of all individual pancreatic voxel BP_{ND} values greater than 0.1 multiplied by the voxel volume (i.e., functional binding capacity) was calculated for each subject. Third, voxel BP_{ND} data were displayed as frequency distribution histograms and compared between the 2 groups.

Statistical Analysis

Descriptive statistics include the arithmetic mean and standard errors of the mean. Least-squares linear regression was used to determine the correlation between outcome measures. The strength of the correlation is expressed in terms of r^2. Student t testing assessed the significance of the difference of means at different BP_{ND} thresholds. All P values are 2-tailed.

RESULTS

Metabolic Testing

Fasting c-peptide concentrations were near or below detection limits (0.15 ng/mL) in plasma of subjects with long-standing type 1 diabetes. Total AUC c-peptide during the mixed-meal tolerance testing in patients was markedly reduced to 2% of control values ($P < 0.001$) (Table 2).

PET Studies

Figure 1 presents the ^{11}C-dihydrotetrabenazine time–activity curves, expressed as standardized uptake value, in the pancreas and left renal cortex of 1 representative control and 1 representative patient. ^{11}C-dihydrotetrabenazine uptake in the pancreas was excellent, peaking at around 10 min (maximum standardized uptake value of 10 and 8 for controls and patients, respectively), with a relatively quick washout for both groups. There was uptake in the renal cortex, peaking early at around 1 min, with a faster washout. These 2 organs thus showed reversible ^{11}C-dihydrotetrabenazine uptake.

In contrast, ^{11}C-dihydrotetrabenazine uptake in the liver increased progressively throughout the study. ^{11}C-dihydrotetrabenazine uptake in the small bowel was slow, with slow washout. The overall time course of ^{11}C-dihydrotetrabenazine uptake in these organs reflected the catabolism of dihydrotetrabenazine by glucuronidation in liver and excretion via bile and urine (*26*). In some subjects, ^{11}C-dihydrotetrabenazine uptake and washout were seen in the gastric antrum. VMAT2 expression has been reported in this tissue (*9*). Cluster analysis–based tissue classification defined the kidney cortex and separated the pancreas from other organs such as the small bowel and stomach (Fig. 2).

Estimation of VMAT2 Binding in Patients and Controls

The pancreatic mean BP_{ND} was decreased in patients (1.86 ± 0.05) to 86% of control values (2.14 ± 0.08) ($P = 0.01$) (Table 2). In controls, but not in patients as expected, the mean BP_{ND} correlated significantly ($r^2 = 0.50$, $P = 0.03$) with AUC c-peptide measures of insulin secretion (Fig. 3). The y-intercept of the regression line had a nonzero BP_{ND} value of 1.504. The functional binding capacity was decreased in patients (44 ± 11) to 40% of control values (109 ± 9) ($P = 0.001$) (Table 2; Fig. 4). The magnitude of decreases in these VMAT2 indices in patients was only moderate despite the fact that all patients had long-standing type 1 diabetes with expected near-total losses of β-cell mass as based on morphometric studies of postmortem pancreata obtained from clinically similar patients. We therefore examined the frequency distribution histograms of pancreatic voxel BP_{ND} and compared them between patients and controls (Figs. 4 and 5, top and bottom panels). The histograms showed that the number of relatively high BP_{ND} voxels was more markedly reduced than was the number of relatively low to moderate BP_{ND} voxels in patients, compared with controls, and corresponded more closely to the known loss of β-cell mass in

TABLE 2. VMAT2 Functional Binding Capacity and AUC C-Peptide Measurements

Subject no.	AUC c-peptide (min × ng/mL)	PET ROI volume (mL)	Mean BPND	VMAT2 functional binding capacity (mL)	
				($BP_{ND} \geq 0.1$)	($BP_{ND} \geq 2.5$)
Controls					
NHDTBZ001	277	72	1.90	148	52
NHDTBZ002	344	56	1.92	115	55
NHDTBZ003	491	59	2.13	132	62
NHDTBZ009	710	44	2.37	109	72
NHDTBZ012	470	51	2.01	108	39
NHDTBZ010	429	25	2.21	59	40
NHDTBZ011	440	42	1.96	82	43
NHDTBZ013	537	40	2.14	91	42
NHDTBZ014	543	51	2.62	140	107
Mean ± SEM	471 ± 41	49 ± 4	2.14 ± 0.08	109 ± 9	57 ± 7
Patients					
NHDTBZ004	19	20	1.66	33	5.8
NHDTBZ005	16	14	1.83	26	8.1
NHDTBZ006	17	34	1.99	68	27
NHDTBZ007	<4.5	28	1.95	55	29
NHDTBZ008	<4.5	42	1.86	78	26
NHDTBZ016	<4.5	5	1.59	8	2.5
Mean ± SEM	11 ± 3	24 ± 5	1.86 ± 0.05	44 ± 11	16 ± 5
t test (P)	<0.001	0.002	0.014	0.001	0.001
Patients/controls (%)	2.3	50	86	40	28

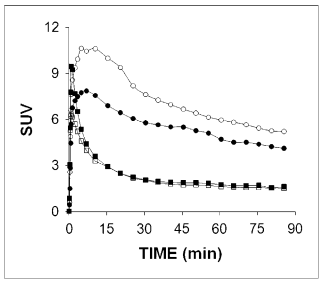

FIGURE 1. Representative time–activity curves of ^{11}C-dihydrotetrabenazine uptake in pancreas and left renal cortex of study subjects. Time–activity curves are shown with circles and squares for pancreas and left renal cortex, respectively, and open and solid symbols indicate 1 control and 1 patient, respectively.

patients. The relative sparing of the voxels with relatively low to moderate BP_{ND} in patients accounted for the only mild to moderate decreases in the mean BP_{ND} values and functional binding capacity ($BP_{ND} > 0.1$) in patients (Fig. 5). The recognition of these findings prompted us to speculate on the possibility that the low to moderate BP_{ND} signal in patients, rather than representing only β-cell mass, might be either due to the higher ^{11}C-dihydrotetrabenazine nonspecific binding in the pancreas than in the renal cortex or due to the presence of non–β-cell VMAT2 binding.

Assuming these possibilities, we recalculated the functional binding capacity using only voxels with values of BP_{ND} greater than 2.5 as a method to remove the contribution of low to moderate BP_{ND} signal assumed to represent nonspecific binding to the total VMAT2 signal. At a threshold BP_{ND} of 2.5, functional binding capacity was more markedly decreased in patients, to 28% of control values (Table 2; Fig. 4, top panel inset). At higher thresholds, there was a greater difference in functional binding capacity between controls and patients but diminishing statistical significance due to the fewer voxels with BP_{ND} greater than 3.0.

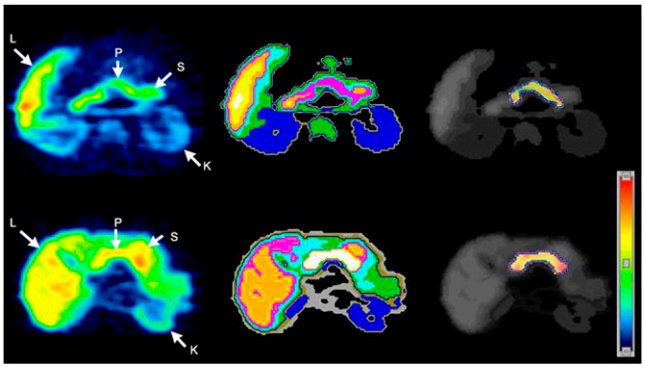

FIGURE 2. Transverse ^{11}C-dihydrotetrabenazine PET images of patients (top row) and controls (bottom row). Summed dynamic PET images were obtained 0–90 min after injection of approximately 481–555 MBq of ^{11}C-dihydrotetrabenazine (left). Corresponding tissue segmentation images are also shown (middle), with different colors being used to represent different organs. Voxelwise parametric images of VMAT2 binding potential (BP_{ND}) are shown (right) using another color scale (right bottom). These BP_{ND} images are fused onto segmentation image using gray scale, with pancreatic ROI boundary shown using dotted blue outlines (right). L = liver; K = kidney; S = stomach; P = pancreas.

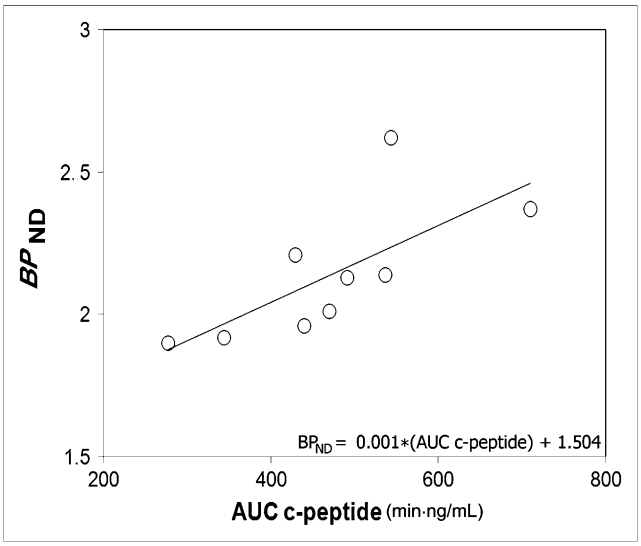

FIGURE 3. Association between binding potential and glucose-stimulated insulin secretion in controls. BP_{ND} values and AUC c-peptide measures for each control were evaluated for strength of association by linear correlation. Regression line (BP_{ND} = 0.001 × AUC c-peptide + 1.504) yielded r^2 of 0.50 and P value of 0.03. x- and y-intercepts were −1.504 and 1.504, respectively.

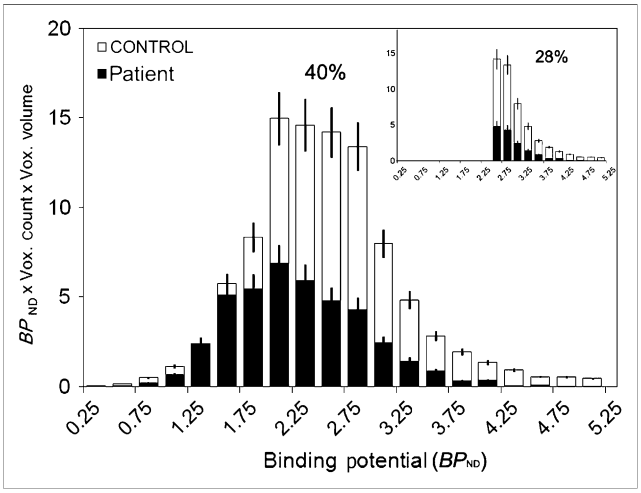

FIGURE 4. VMAT2 functional binding capacity of controls and patients. This histogram plots product of BP_{ND} and voxel (Vox.) volume at each BP_{ND} interval for controls and patients. Functional binding capacity is sum of all columns for each population. Percentage functional binding capacity of patients relative to controls is shown above histogram. Inset shows another histogram considering only BP_{ND} values greater than 2.5 as representative of β-cell mass. Percentage functional binding capacity of patients relative to controls is also shown. Error bars represent SEM.

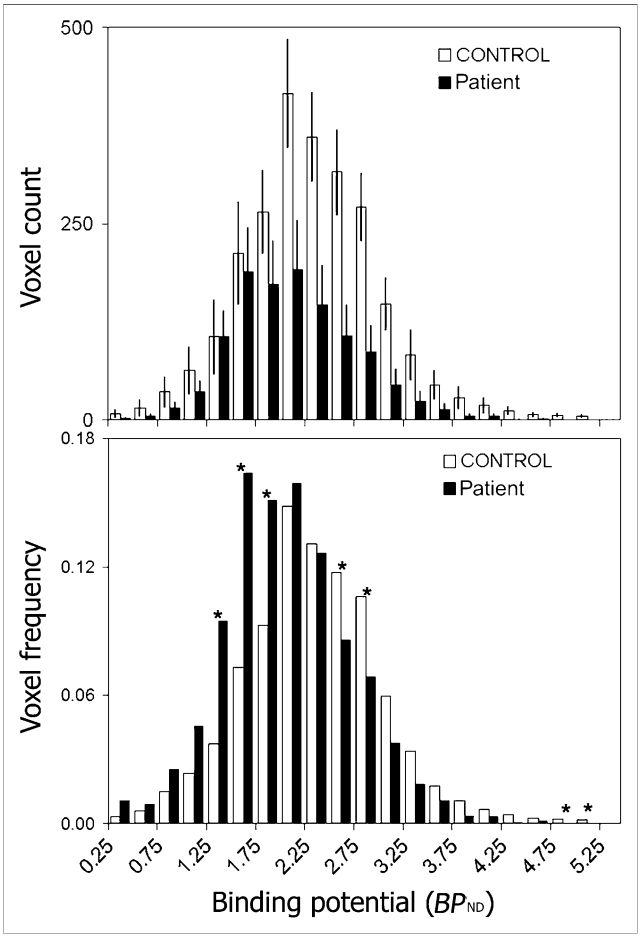

FIGURE 5. Histogram summary of voxel BP_{ND} in controls and patients. (Top) Average number of voxels at each BP_{ND} interval is displayed for controls (n = 9) (white bars) and patients (n = 6) (black bars). Error bars represent SEM. (Bottom) Number of voxels at each BP_{ND} interval was normalized to total number of voxels in ROI for each individual and displayed as mean for controls and patients (i.e., this is a frequency histogram). Asterisks indicate statistically significant differences ($P < 0.05$, Student t test) between controls and patients.

For MRTM2 parametric imaging of BP_{ND} and R_1, the reference tissue clearance rate (left renal cortex), k_2', was estimated by MRTM2. The k_2' values did not differ (P = 0.4) between patients (0.29 ± 0.06 min^{-1}) and controls (0.26 ± 0.08 min^{-1}), and the ratio k_2'/k_2 was 4.4 ± 1.4 (range, 3.2–9.1), where k_2 is the tissue radioligand clearance from the pancreas. The major factors that affect the accuracy of k_2' by MRTM2 are the magnitude of k_2' and the ratio k_2'/k_2 (*23*). These results indicated that the potential bias and variability of MRTM2 estimation of k_2' was small (less than a few percentage points).

In 4 controls with arterial plasma metabolite–corrected input function, comparison of kinetic analysis BP_{ND}, which requires arterial input function, and MRTM2 BP_{ND}, which requires no arterial input function, showed that MRTM2 somewhat overestimated kinetic analysis (percentage differences between the 2 BP_{ND} estimations of +7.5% ± 4.5%). However, linear correlations were strong between kinetic analysis BP_{ND} and MRTM2 BP_{ND}, with an r^2 of 0.89 ± 0.01 (range, 0.88–0.91).

DISCUSSION

Measurements of stimulated c-peptide and insulin secretion have been used to monitor changes in β-cell mass. However, none of these approaches is capable of providing direct measures of β-cell mass. Previous feasibility studies on rodents suggested that PET-based measurements of VMAT2 densities in the pancreas might be used as a biomarker of β-cell mass (*17*).

In this ^{11}C-dihydrotetrabenazine PET study, we attempted to quantify pancreatic VMAT2 binding in a cross-sectional study of healthy volunteers and patients with long-standing type 1 diabetes. In contrast to the findings of the ^{11}C-dihydrotetrabenazine PET studies of a rodent model of type 1 diabetes (*17*), the results of our human study suggest the presence of a substantial amount of VMAT2 binding signal in the type 1 diabetic pancreas. The mean pancreatic BP_{ND} in patients was decreased by only 14%. The voxel BP_{ND} histogram showed that voxels with low to moderate BP_{ND} were relatively spared in patients. The functional binding capacity with consideration of only BP_{ND} greater than 2.5 was markedly reduced by 72% in patients. However, there was still a significant amount of VMAT2 binding signal, even expressed as functional binding capacity ($BP_{ND} > 2.5$) (28% of control values), in patients despite postmortem evidence that loss of β-cell mass is nearly total in long-standing type 1 diabetes (*27*).

The results of the current human study then raise 2 questions: Why is there a VMAT2 binding signal in type 1 diabetic pancreata, and why are the results of the current study different from those of previous rodent studies?

Several nonexclusive explanations exist for the presence of VMAT2 binding signal in our human type 1 diabetic pancreata. First, in our analysis, the renal cortex was used to estimate dihydrotetrabenazine nonspecific binding in the pancreas because VMAT2 expression is undetectable in the renal cortex and ^{11}C-dihydrotetrabenazine is a highly selective ligand for VMAT2 (*10,13*). However, the nonspecific ^{11}C-dihydrotetrabenazine binding may be greater in the human pancreas than in the renal cortex because of differences in cellular composition of the tissue, for example (*28*). Should this be the case, our actual BP_{ND} may overestimate the true BP_{ND} of the pancreata. That is, our assumption that V_{ND} equals V'_{ND} may not be valid. This overestimation of BP_{ND} due to the underestimation of the pancreatic nonspecific binding may represent the majority of the VMAT2 binding signal in type 1 diabetic pancreata in this report. However, if this positive bias of BP_{ND} is systematic (i.e., BP_{ND} is linearly proportional to β-cell mass), our VMAT2 binding measurements may be an index of β-cell mass, although the sensitivity of detecting changes in β-cell mass may be reduced.

In the present study, we chose the renal cortex because no other organs within the field of view were suitable for use as the reference tissue. Other tissues, such as the oxyntic stomach, express VMAT2. Liver is the site of metabolism and excretion of ^{11}C-dihydrotetrabenazine, and the bowel contains radioactive bile. The adjacent muscle and soft-tissue volumes were too small to provide adequate sampling of ^{11}C-dihydrotetrabenazine activity. Although the left renal cortex was suitable for the reference tissue in the MRTM2 analysis, this organ may not be optimal for estimating nonspecific binding in the pancreas, because the kinetics of ^{11}C-dihydrotetrabenazine uptake in the kidney may be complex (*26*).

Use of metabolite-corrected plasma instead of the reference tissue as an input function allows estimation of nonspecific (V_{ND}) and specific (V_S) distribution volumes separately in the pancreas. However, the V_{ND} or V_S estimated by this method is generally unreliable, although estimates of the total distribution volume ($V_T = V_{ND} + V_S$) are reliable. Therefore, even with plasma data, V_{ND} is often constrained to the value of the reference tissue (V'_{ND}) to estimate V_S if such reference tissue exists. Therefore, to validate the use of the renal cortex as the reference tissue, one must estimate nonspecific binding in the pancreas by using alternate experimental approaches.

One such approach would be to block ^{11}C-dihydrotetrabenazine binding with cold dihydrotetrabenazine in sufficient doses to block VMAT2 binding sites completely. In rodent experiments, cold dihydrotetrabenazine (2 mg/kg) displaces 35%−40% of the signal of the average standardized uptake value time–activity curve (60–120 min) for the pancreas and suggests that nonspecific binding of ^{11}C-dihydrotetrabenazine in the pancreas is underestimated by 12% when the kidney cortex is used as a reference (*14*). However, this approach is not clinically applicable because of the side effects of blocking the VMAT sites in the central nervous system by the necessary pharmacologically active doses of dihydrotetrabenazine.

Another potentially confounding source of the VMAT2 signal are the radioactive metabolites of ^{11}C-dihydrotetrabenazine that may enter the pancreas because the blood–brain barrier has no counterpart in the pancreas. This possibility could complicate quantifications using metabolite-corrected plasma input function. In the present study, the contribution of radioactive metabolites was assumed negligible. However, in future studies, this metabolite issue needs to be evaluated. In addition, radioactive metabolites are excreted into bile that empties via the common duct and sphincter of Oddi into the duodenum at the head of the pancreas. This contamination by bile activity may contribute to a VMAT2 signal in the head of pancreas near the sphincter of Oddi. In future studies, this potential bile contamination also needs to be addressed.

Yet another origin of the residual signal in type 1 diabetic pancreata might be VMAT2 expressed within the pancreas but not associated with the β-cell mass (e.g., neuronal cells or immature β-cells). A recent examination of postmortem pancreas tissue, representing pancreata studied here, showed a linear correlation between VMAT2 and insulin expression in both health and disease, as well as a minor population of VMAT2-positive but insulin-negative cells (<1% total VMAT2-positive cell area) (Saisho et al., unpublished data).

The second question generated by this initial human study is why the magnitude of the PET signal in type 1 diabetic pancreata differs from our previous findings in rodent models of diabetes (*17*). The differences in radioligand uptake may be related to differences in nonspecific binding of ^{11}C-dihydrotetrabenazine between the species, the duration of disease, or inaccuracies of quantitation in the rodent model due to slower kinetics of pancreatic tracer uptake and washout or receptor saturation (*29*). A complete explanation for the differences requires further study.

As predicted from studies of β-cell mass in animal models, our primary outcome measure, BP_{ND}, correlated significantly with the β-cell functional measure AUC c-peptide in controls but not in patients. The PET volumes were consonant with previous measurements of pancreata (*30*), and, similar to already published reports (*31*) and as expected, pancreatic PET volumes did not correlate with AUC c-peptide. The total pancreatic VMAT2 functional binding capacity was substantially less in patients than in controls, confirming our working hypothesis, although the decreases were underestimated. Our voxelwise analysis of ^{11}C-dihydrotetrabenazine binding in our study population suggests that the reduction in pancreas volume alone did not fully account for the loss in functional VMAT2 binding capacity observed in the type 1 diabetes population. This suggestion arises from 2 observations: a reduction in the average BP_{ND} in type 1 diabetic pancreata relative to control pancreata, and a 72% loss of functional binding capacity in type 1 diabetic pancreata, with a BP_{ND} of 2.5 or greater surpassing the 50% loss of the PET-measured pancreas volume.

Our experience with rodent models of diabetes, as well as our understanding of the natural variability in β-cell mass (3- to 5-fold differences among individuals of similar age or body mass index) (*32*), suggests that the potential clinical value of this technique will lie in longitudinal, rather than cross-sectional, studies in which changes in β-cell mass are evaluated to predict the onset of diabetes or to assess strategies to preserve β-cell mass. If validated in longitudinal studies of human new-onset diabetes, PET measurements of VMAT2 binding capacity within the pancreas may be a useful biomarker for β-cell mass. In our future studies, however, we may choose to take advantage of novel ^{18}F-analogs of dihydrotetrabenazine that appear to possess higher VMAT2 affinities and lower nonspecific binding, in addition to the advantage of the longer physical half-life of ^{18}F (*14*).

CONCLUSION

These results suggest that ^{11}C-dihydrotetrabenazine PET allows quantification of VMAT2 binding in the human

pancreas. However, BP_{ND} and functional binding capacity appear to overestimate the β-cell mass in view of the known near-complete depletion of β-cell mass in long-standing type 1 diabetes, which may be due to higher nonspecific binding in the pancreas than in the renal cortex. Further studies are warranted to address this possible overestimation of VMAT2 binding in the pancreas.

ACKNOWLEDGMENTS

This work was supported by the PHS, NIH, NIDDK, 1 RO1 DK077493(PEH), and funds provided by the Naomi Berrie Diabetes Center. We thank the study participants and acknowledge the significant contributions of Chitra Saxena, Arthur Mikno, Michael D. Farwell, Monica Chung, Steven Dashnaw, Sara Plett, Kevin Desimone, Cyrill Burger, Raj Murthy, Debora Kessler, and research coordinators Pat Kringas and Ellen Greenberg.

REFERENCES

1. Kloppel G, Drenck CR, Oberholzer M, Heitz PU. Morphometric evidence for a striking B-cell reduction at the clinical onset of type 1 diabetes. *Virchows Arch.* 1984;403:441–452.
2. Butler AE, Galasso R, Meier JJ, Basu R, Rizza RA, Butler PC. Modestly increased beta cell apoptosis but no increased beta cell replication in recent-onset type 1 diabetic patients who died of diabetic ketoacidosis. *Diabetologia.* 2007;50:2323–2331.
3. McCulloch DK, Koerker DJ, Kahn SE, Bonner-Weir S, Palmer JP. Correlations of in vivo beta-cell function tests with beta-cell mass and pancreatic insulin content in streptozocin-administered baboons. *Diabetes.* 1991;40:673–679.
4. Dotta F, Censini S, van Halteren AG, et al. Coxsackie B4 virus infection of beta cells and natural killer cell insulitis in recent-onset type 1 diabetic patients. *Proc Natl Acad Sci USA.* 2007;104:5115–5120.
5. Wajchenberg BL. β-Cell failure in diabetes and preservation by clinical treatment. *Endocr Rev.* 2007;28:187–218.
6. Tsai EB, Sherry NA, Palmer JP, Herold KC. The rise and fall of insulin secretion in type 1 diabetes mellitus. *Diabetologia.* 2006;49:261–270.
7. Weir GC, Bonner-Weir S. Five stages of evolving beta-cell dysfunction during progression to diabetes. *Diabetes.* 2004;53(suppl 3):S16–S21.
8. Vander Borght T, Kilbourn M, Desmond T, Kuhl D, Frey K. The vesicular monoamine transporter is not regulated by dopaminergic drug treatments. *Eur J Pharm.* 1995;294:577–583.
9. Anlauf M, Eissele R, Schafer MK, et al. Expression of the two isoforms of the vesicular monoamine transporter (VMAT1 and VMAT2) in the endocrine pancreas and pancreatic endocrine tumors. *J Histochem Cytochem.* 2003;51:1027–1040.
10. Maffei A, Liu Z, Witkowski P, et al. Identification of tissue-restricted transcripts in human islets. *Endocrinology.* 2004;145:4513–4521.
11. Raffo A, Hancock K, Polito T, et al. Role of vesicular monoamine transporter type 2 in rodent insulin secretion and glucose metabolism revealed by its specific antagonist tetrabenazine. *J Endocrinol.* 2008;198:41–49.
12. Erickson JD, Schafer MK, Bonner TI, Eiden LE, Weihe E. Distinct pharmacological properties and distribution in neurons and endocrine cells of two isoforms of the human vesicular monoamine transporter. *Proc Natl Acad Sci USA.* 1996;93:5166–5171.
13. Scherman D, Raisman R, Ploska A, Agid Y. [^{3}H]dihydrotetrabenazine, a new in vitro monoaminergic probe for human brain. *J Neurochem.* 1988;50:1131–1136.
14. Kung MP, Hou C, Lieberman BP, et al. In vivo imaging of beta-cell mass in rats using ^{18}F-FP-(+)-DTBZ: a potential PET ligand for studying diabetes mellitus. *J Nucl Med.* 2008;49:1171–1176.
15. DaSilva JN, Kilbourn MR. In vivo binding of [^{11}C]tetrabenazine to vesicular monoamine transporters in mouse brain. *Life Sci.* 1992;51:593–600.
16. Bohnen NI, Albin RL, Koeppe RA, et al. Positron emission tomography of monoaminergic vesicular binding in aging and Parkinson disease. *J Cereb Blood Flow Metab.* 2006;26:1198–1212.
17. Simpson NR, Souza F, Witkowski P, et al. Visualizing pancreatic beta-cell mass with [^{11}C]DTBZ. *Nucl Med Biol.* 2006;33:855–864.
18. Kilbourn M, Lee L, Vander Borght T, Jewett D, Frey K. Binding of alpha-dihydrotetrabenazine to the vesicular monoamine transporter is stereospecific. *Eur J Pharm.* 1995;278:249–252.
19. Parsey RV, Ojha A, Ogden RT, et al. Metabolite considerations in the in vivo quantification of serotonin transporters using ^{11}C-DASB and PET in humans. *J Nucl Med.* 2006;47:1796–1802.
20. Koeppe RA, Frey KA, Vander Borght TM, et al. Kinetic evaluation of [^{11}C]dihydrotetrabenazine by dynamic PET: measurement of vesicular monoamine transporter. *J Cereb Blood Flow Metab.* 1996;16:1288–1299.
21. Pick A, Clark J, Kubstrup C, et al. Role of apoptosis in failure of beta-cell mass compensation for insulin resistance and beta-cell defects in the male Zucker diabetic fatty rat. *Diabetes.* 1998;47:358–364.
22. Ichise M, Liow JS, Lu JQ, et al. Linearized reference tissue parametric imaging methods: application to [^{11}C]DASB positron emission tomography studies of the serotonin transporter in human brain. *J Cereb Blood Flow Metab.* 2003;23:1096–1112.
23. Ichise M, Cohen RM, Carson RE. Noninvasive estimation of normalized distribution volume: application to the muscarinic-2 ligand [^{18}F]FP-TZTP. *J Cereb Blood Flow Metab.* 2008;28:420–430.
24. Kim JS, Ichise M, Sangare J, Innis RB. PET imaging of serotonin transporters with [^{11}C]DASB: test-retest reproducibility using a multilinear reference tissue parametric imaging method. *J Nucl Med.* 2006;47:208–214.
25. Kim J, Cai W, Feng D, Eberl S. Segmentation of VOI from multidimensional dynamic PET images by integrating spatial and temporal features. *IEEE Trans Inf Technol Biomed.* 2006;10:637–646.
26. Mehvar R, Jamali F, Watson MW, Skelton D. Pharmacokinetics of tetrabenazine and its major metabolite in man and rat: bioavailability and dose dependency studies. *Drug Metab Dispos.* 1987;15:250–255.
27. Meier JJ, Bhushan A, Butler AE, Rizza RA, Butler PC. Sustained beta cell apoptosis in patients with long-standing type 1 diabetes: indirect evidence for islet regeneration? *Diabetologia.* 2005;48:2221–2228.
28. de Vries EF, van Waarde A, Buursma AR, Vaalburg W. Synthesis and in vivo evaluation of ^{18}F-desbromo-DuP-697 as a PET tracer for cyclooxygenase-2 expression. *J Nucl Med.* 2003;44:1700–1706.
29. Jagoda EM, Vaquero JJ, Seidel J, Green MV, Eckelman WC. Experiment assessment of mass effects in the rat: implications for small animal PET imaging. *Nucl Med Biol.* 2004;31:771–779.
30. Williams AJ, Chau W, Callaway MP, Dayan CM. Magnetic resonance imaging: a reliable method for measuring pancreatic volume in type 1 diabetes. *Diabet Med.* 2007;24:35–40.
31. Nyren S, Blomqvist L, Efendic S, Grill V. Pancreas size and insulin secretion: lack of association in non-diabetic subjects. *Acta Diabetol.* 1996;33:274–276.
32. Meier JJ, Butler AE, Saisho Y, et al. Beta-cell replication is the primary mechanism subserving the postnatal expansion of beta-cell mass in humans. *Diabetes.* 2008;57:1584–1594.